4022–4032 *Nucleic Acids Research, 2009, Vol. 37, No. 12* *Published online 05 May 2009*
doi:10.1093/nar/gkp284

One RNA aptamer sequence, two structures: a collaborating pair that inhibits AMPA receptors

Zhen Huang[1], Weimin Pei[1], Yan Han[1], Sabarinath Jayaseelan[1], Alexander Shekhtman[1], Hua Shi[2] and Li Niu[1,*]

[1]Department of Chemistry and Center for Neuroscience Research and [2]Department of Biological Sciences, University at Albany, SUNY, Albany, NY 12222, USA

Received October 7, 2008; Revised April 11, 2009; Accepted April 14, 2009

ABSTRACT

RNA is ideally suited for *in vitro* evolution experiments, because a single RNA molecule possesses both genotypic (replicable sequence) and phenotypic (selectable shape) properties. Using systematic evolution of ligands by exponential enrichment (SELEX), we found a single 58-nt aptamer sequence that assumes two structures with different functions, both of which are required to inhibit the GluR2 AMPA receptor channel. Yet, the two structures, once formed during transcription, appear to be incapable of interconverting through unfolding and refolding, presumably due to their extraordinary structural stability. Thus, our results suggest more broadly that natural RNA molecules can evolve to acquire alternative structures and associated functions. Such divergence of RNA phenotype may precede gene duplication at the genome level.

INTRODUCTION

Both theoretical (1) and experimental (2) work demonstrated that a single RNA sequence can assume multiple, distinctly folded structures with different functions. These structures, or more precisely conformations, are different structural folds of the same sequence generated through reversible thermodynamic pathways. For example, a selected RNA sequence can adopt a fold that catalyzes RNA cleavage or a different fold that catalyzes RNA ligation (2). On binding of small metabolites, riboswitches can switch their conformations and consequently functions (3). However, here we describe that a single RNA sequence assumes two structures with different functions, both of which are required to work together in order to inhibit the GluR2 AMPA receptor. Yet, the two structures, once formed during transcription, are not interconvertible through unfolding and refolding or refolding after denaturation.

The sequence we present corresponds to an aptamer, which we termed as AN58. AN58 was derived from its predecessor RNA of 99-nt (i.e. aptGluR2-99) by sequence reduction, and aptGluR2-99 was evolved from systematic evolution of ligands by exponential enrichment (SELEX) (4,5) against the GluR2 receptor (6) from an RNA library containing $\sim 10^{15}$ sequences. AN58 is a minimal, functional aptamer, compared to aptGluR2-99, whereas RNAs shorter than the 58-nt sequence, such as 53 nt (five more base deletion from the 3′-end of AN58), lost all inhibitory activities against GluR2 (6). GluR2 is one of the α-amino-3-hydroxy-5-methyl-4-isoxazole propionic acid (AMPA) receptor subunits of the glutamate ion channel family, and it plays a key functional role in brain activities such as learning and memory (7,8). Excessive activity of the GluR2 AMPA receptors has been implicated in a number of neurological diseases, and therefore aptamers as inhibitors might be useful as pharmacological tools (8).

MATERIALS AND METHODS

Transcription and purification of M1 and M2

The enzymatic transcription reaction of the AN58 DNA template generated two RNA species, which we termed as M1 and M2. The *in vitro* transcription was carried out using the MEGAshortscript T7 transcription kit (Ambion) with a 1:1 mixture of the single stranded DNA template synthesized based on the complementary sequence of AN58 and the T7 promoter oligo, i.e. 5′-TAA TACGACTCACTATA-3′. The M1 and M2 were separated from the transcription reaction mixture in a Prep Cell polyacrylamide gel electrophoresis (PAGE) column (Bio-Rad) and were individually passed through a Q column (Bio-Rad) to remove polyacrylamide bound to RNA samples, as monitored in NMR (6). The pooled sample was then dialyzed against an appropriate buffer, such as the external buffer for electrophysiology (150 mM NaCl, 3 mM KCl, 1 mM $CaCl_2$, 1 mM $MgCl_2$, 50 mM HEPES, pH 7.4), and concentrated using an Amicon

*To whom correspondence should be addressed. Tel: +1 518 591 8819; Fax: +1 518 591 8820; Email: lniu@albany.edu

Ultra centrifugal filter (Millipore). It should be emphasized that the purification of M1 and M2, described above, was necessary to ensure that the inability of interconversion between M1 and M2 (as shown in Figure 4A) was not due to the presence of acrylamide bound to these RNA molecules, causing an artificial stabilization of M1 and M2 in the folding/refolding experiments.

Transcription and purification of AN59 M1 and AN59 M2 by using *glmS* ribozyme

To create an even 3′-end of M1 and M2 species by *in vitro* transcription reaction, we cloned AN58 DNA sequence into pRAV23 vector (9) that contains the sequence of the *glmS* ribozyme (10). In our construct, the AN58 DNA sequence was ligated into the *EcoR* I (5′-) and *Kpn* (3′-) sites, respectively, and the AN58 sequence was inserted upstream of the *glmS* sequence with an additional nucleotide A. The *glmS* ribozyme cleaved the RNA sequence at the AG site upstream at its 3′-end, releasing a single, cleavage fragment (10). Therefore, the constructed plasmid was linearized and used as the template for *in vitro* transcription of AN59 M1 and AN59 M2. After transcription reaction by using the MEGAshortscript T7 RNA kit, the transcription product was incubated with 1 mM glucosamine-6-phosphate (Sigma), a metabolite that accelerates the cleavage reaction, for 2 h in a buffer containing 50 mM Tris–HCl (pH 7.4), 10 mM $MgCl_2$ and 200 mM KCl. The reaction mixture, which contained AN59 M1/M2, was separated through a PAGE column and further purified by passing through a Q column, as described above for the AN58 M1/M2 purification.

Modification of RNA with glyoxal and characterization of the glyoxalation products

To evaluate the electrophoretic mobility of AN58 M1 and M2 without interference of base paring, we treated M1 and M2 with glyoxal (11). Glyoxalation introduces a bulky adduct into guanosine residues, which then sterically hinders GC-pair formation (11). Experimentally, 100 ng of an RNA sample in 5 µl was mixed with equal volume of glyoxal loading buffer (supplied by Applied Biosystems/Ambion and it contained glyoxal, DMSO, ethidium bromide and bromophenol blue). The mixture was incubated at 50°C for 1 h. After incubation, the sample was kept on ice before loading on a 1 × 3-morpholinopropanesulfonic acid (MOPS) buffered, 10% native PAGE. The electrophoresis was run in 1 × MOPS buffer at a constant voltage of 5 V/cm (12). The gel was stained by using SYBR Gold (Invitrogen) and visualized under UV illumination.

Primer extension

A 10-nt oligo (i.e. 5′-GGACGAAACT-3′) complementary to the 3′-end of AN58 was 5′-^{32}P-labeled using [γ-^{32}P]ATP with T4 polynucleotide kinase (Ambion). The cDNA was synthesized by using a primer extension reaction containing 1.25 mM of each dNTP (GCAT), 5 mM DTT and 200 units of Superscript III reverse transcriptase (Invitrogen). The mixture was first treated with RNase H (New England Biolabs) and was loaded on an 8% polyacrylamide sequencing gel containing 8 M urea. The radioactivity of a reverse transcription (RT) reaction was detected by exposing the gel to a phosphorimage screen (GE Healthcare), which was digitized in a PhosphorImager (Typhoon Trio, GE Healthcare). The intensity of the radioactivity was quantified by using ImageQuant TL (GE Healthcare).

Dideoxy-mediated RNA sequencing

A 15-nt oligo (5′-GGACGAAACTTGTCC-3′) complementary to the 3′-end of AN58 was 5′-^{32}P-labeled using [γ-^{32}P]ATP as described in Primer Extension. The dideoxy-mediated RT reaction consisted of 5 pmol RNA, 0.5 pmol of 15-nt oligo, 25% dimethyl sulfoxide (DMSO), 50 mM Tris–HCl (pH 8.3), 40 mM KCl, 8 mM $MgCl_2$, 1 mM dithiothreitol, 0.75 mM dNTP and 0.225 mM ddNTP. The reaction was carried out in the presence of an enhanced avian reverse transcriptase (Sigma) at 42°C for 1 h. The sample was treated using RNase H (New England Biolabs) and run through a sequencing PAGE gel. The sequence was visualized through the radioactivity as described above and was confirmed using the synthetically made AN58 or SynAN58 whose sequence was known (Trilink Biotechnologies, San Diego, CA).

In-line probing

RNA samples used for in-line probing were purified by running through an XBridge C18 column (Waters) on a Waters Breeze HPLC system, and the column was maintained at 55°C throughout the purification. The running buffer contained 5% methanol in triethylamine/hexafluoroisopropanol solution (TEA/HFIP, 16.3 mM/400 mM, pH 7.9). A sample was eluted using the same buffer but with a linear gradient of increasing methanol concentration up to 30%. A purified RNA sample was 5′-^{32}P-labeled using [γ-^{32}P]ATP and was purified through a 10% native PAGE. The RNA sample obtained from the gel was ethanol precipitated, air dried and re-dissolved in 10 mM Tris–HCl buffer (pH 7.4). SynAN58 RNA was used as the control, which was prepared in the same way. The in-line probing experiments were carried out by the following procedure. Samples were mixed with external buffer (note that the pH was adjusted to pH 8.6) and kept at 37°C for up to 72 h. The samples were then ethanol precipitated, air dried, and re-dissolved in 5 mM Tris–HCl buffer containing 47.5% formamide. All of the samples were loaded onto a 12% sequencing PAGE containing 8 M urea. The gel was dried, which was then exposed to a phosphorimage screen. The image was captured by a phosphorimage scanner and analyzed by ImageQuant TL.

Selective 2′-hydroxyl acylation analyzed by primer extension (SHAPE)

SHAPE experiments were carried out to probe the structures of M1, M2 and SynAN58. For the SHAPE experiment, an RNA sample was dissolved in 10 mM Tris buffer, and the salt concentration was adjusted to (in mM) 150 NaCl, 3 KCl, 1 $CaCl_2$, 1 $MgCl_2$, 10 HEPES (pH 7.4).

The sample was heated to 95°C for 3 min, placed on ice for 1 min and then was left at 37°C for 30 min. *N*-Methylisatoic anhydride (NMIA) dissolved in DMSO was added to the sample, which reacted with the 2′-hydroxyl group of a ribose, generating a corresponding ester adduct (13). The NMIA reaction was run at 37°C for 50 min. The sample was then ethanol precipitated, air-dried and re-dissolved into dH_2O for primer extension. The primer extension reaction was run by the method described earlier, except that a 15-nt oligo, 3P15 (5′-GG ACGAAACTTGTCC-3′), was used.

Receptor expression

The homomeric $GluR2Q_{flip}$ AMPA receptor channel was transiently expressed in human embryonic kidney (HEK)-293S cells as described (14). The cells were maintained in Dulbecco's modified Eagle's medium supplemented with 10% fetal bovine serum, in a 37°C, 5% CO_2, humidified incubator. The cells were used for electrophysiology from 48 h after transfection.

Electrophysiology

The inhibitory function of an aptamer was measured using whole-cell recording, as described previously (6,15). Briefly, the electrode had a resistance of ~3 MΩ after it was filled with the electrode solution (in mM): 110 CsF, 30 CsCl, 4 NaCl, 0.5 $CaCl_2$, 5 EGTA, and 10 HEPES (pH 7.4 adjusted by CsOH). All reagents, including aptamers and glutamate, were dissolved in the external buffer and used for whole-cell recording. The external buffer composition was described earlier in purification of M1 and M2 of the 'Materials and methods' section. A solution flow device (14) was used to apply glutamate in the absence and presence of an aptamer to an HEK-293 cell expressing the receptor. Glutamate-induced whole-cell current was recorded at −60 mV and 22°C. Unless noted otherwise, each data point in Figure 1C and 1D was an average of at least three measurements collected from at least three cells. Origin 7 was used for data analysis and plotting. Uncertainties reported refer to standard deviation from the mean.

RESULTS

Different functional roles of M1 and M2

We previously showed that RNA aptamer AN58 and its longer versions were all potent inhibitors of GluR2 AMPA receptors (6). In a native PAGE (Figure 1A), AN58 and its longer versions exhibited two or more than two bands. Surprisingly, however, the two bands of AN58, generated by *in vitro* transcription and labeled as M1 and M2 in Figure 1A, did not individually inhibit the GluR2 receptor, as characterized by whole-cell recording of the GluR2 receptor channel expressed in HEK-293 cells (14) (Figure 1B). Yet, when mixed with equal molar ratio, M1 and M2 inhibited the receptor as fully as they did before they were separated (Figure 1C).

More surprisingly, M1 and M2 were found to have different functional roles in inhibiting the GluR2 receptor, a conclusion drawn from a series of whole-cell current recording experiments (Figure 1D). First, an equal molar mixture of the non-inhibitory 53-nt transcript (AN53) with the purified M2 yielded no inhibition, but the mixture of the 53-nt transcript with the purified M1 produced an inhibition as strong as the mixture of purified M1 and M2 (Figure 1D). As a control, RN87 whose RNA sequence is different from either AN58 or AN53 showed no inhibition itself or when mixed with either M1 or M2 (Figure 1D). These results (Figures 1C and D) indicated that M1 and M2 functioned differently, by binding separately to two different sites, but M1 and M2 were required to act as a collaborating pair to inhibit GluR2 (Figure 1E). We previously concluded that AN58 was a competitive inhibitor based on the fact that the original sequence of AN58 was evolved from SELEX using 6-nitro-7-sulfamoylbenzo[f]quinoxaline-2,3-dione (NBQX) as the selection pressure to displace aptamers from their binding sites or a site that was mutually exclusive (6), and that the NBQX is a classic competitive inhibitor of the AMPA/kainate subtypes of glutamate receptors (16). Furthermore, AN58 was shown to displace NBQX bound to the receptor in a radio-ligand binding assay and also to right-shift the dose-response curve established by whole-cell current recording (6). Based on this mechanism of the collective action of M1 and M2 (Figure 1E), the intrinsic inhibition constant or K_I for M1 and M2 was estimated to be 25 ± 4 and 27 ± 7 nM, respectively (Supplementary Figure 1). The experiment using different ratios of M1 and M2 further revealed that the relative stoichiometry of the inhibition was 1:1 (Supplementary Figure 1).

Sequencing of M1 and M2

Based on the finding that M1 and M2 had different functional roles but had to act together in order to inhibit the receptor (Figure 1C and D), we hypothesized that the functional difference between M1 and M2 was a result of different structures assumed from the same sequence. To test this hypothesis, we first sequenced M1 and M2 by primer extension, using the synthetically made AN58 or SynAN58 with the known sequence as the ladder. As expected, the sequence of M1 and M2 was identical (Supplementary Figure 2) (note that the 3′-end sequence was not resolved due to the annealing of a 15-nt primer for the sequencing). Using either a 12-nt or 17-nt primer annealed at the 3′-end also produced the same sequencing information for M1 and M2 (data not shown). We further demonstrated that M1 and M2, once chemically modified by glyoxal, were able to migrate with the same mobility (Figure 2A) in PAGE, suggesting that M1 and M2 also had the same length. The use of glyoxal to completely denature RNAs by glyoxalating their bases, thus prohibiting base pairing, allowed RNAs to migrate in PAGE without interference of secondary structures (11).

Structural differences in M1, M2 and SynAN58

Evidence that M1 and M2 had the same length, resolved in glyoxal/PAGE (Figure 2A), and the same sequence, revealed by primer extension (Supplementary Figure 2),

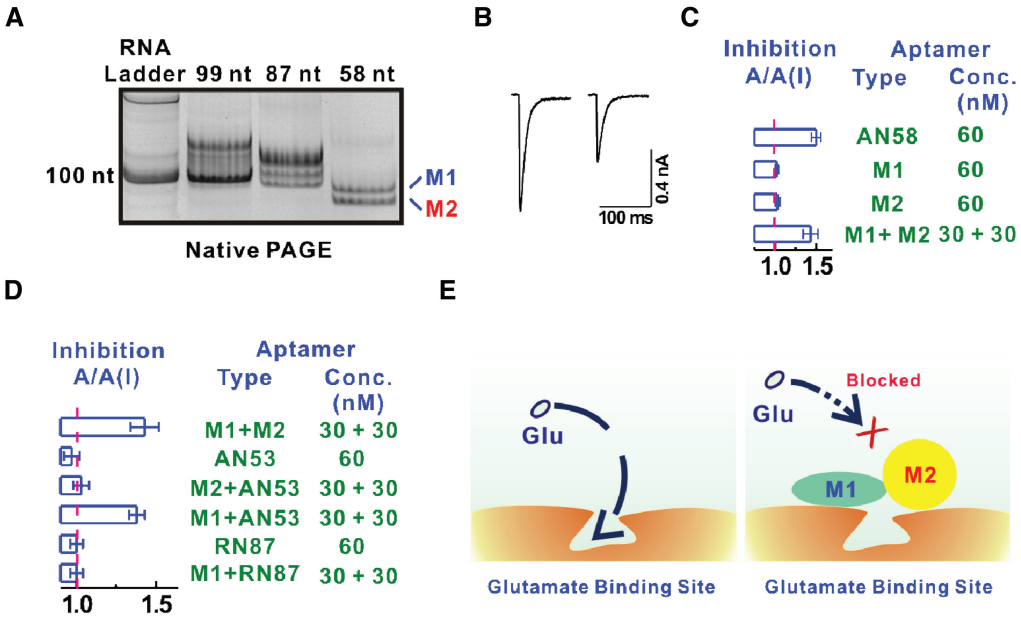

Figure 1. Different functional (inhibitory) roles of M1 and M2. (**A**) M1 and M2 derived from AN58 were visualized in native PAGE (10%) by ethidium bromide staining, together with its longer versions, i.e. 87-nt and 99-nt (i.e. aptGluR2-99) aptamers. RNA Century marker (Applied Biosystem) was loaded in the first lane and the lowest band corresponded to 100-nt length. (**B**) Representative whole-cell current response of $GluR2Q_{flip}$ expressed in HEK-293 cells to 500 μM glutamate in the absence (left panel) and presence (right panel) of 30 nM AN58 (unless otherwise noted, 500 μM glutamate was used for all the assays in this study). (**C**) M1 or M2 alone caused no inhibition but an equal molar mixture of M1 and M2 restored the inhibition of GluR2 to the same level by the non-separated AN58 at identical concentrations. (**D**) Mixing of AN53 with M1, but not M2, yielded inhibition, but AN53 alone did not inhibit the receptor. As a control, the mixture of M1 and another non-functional RNA, RN87, caused no inhibition. (**E**) As a competitive inhibitor pair, M1 and M2 are proposed to bind to their corresponding sites simultaneously and in 1:1 stoichiometry ratio (see Supplementary Figure 1) to block the entry of glutamate to its binding site.

but exhibited different electrophoretic mobility in both native (Figures 1A and 2A) and denatured PAGE (Figure 4A) suggested that M1 and M2 had different secondary and perhaps tertiary structures. Indeed, the primer extension reaction by using the same 3′-end primer revealed a difference in the reverse transcription or RT pattern between M1 and M2 (Figure 2B). The existence of intermediate RT stops or pauses during elongation of reverse transcription, like those observed here, is known to be induced by structured regions in an RNA template (17,18). As such, the different RT pause patterns at various nucleotide positions between M1 and M2 supported the notion that M1 and M2 assumed two distinct structures from the same sequence (see the bar chart in Figure 2B).

We further preformed in-line probing experiment with M1 and M2, using SynAN58 as a control (Figure 2C). The in-line probing experiment was useful because it directly revealed the precise nucleotide positions that define the structural differences between M1 and M2 even possibly in the last 15-nt region that was not observable in primer extension experiments, such as in the RT stop patterns (or Figure 2B). In-line probing experiment is based on the inherent intramolecular phosphoester transfer or transesterification reaction of an RNA due to a nucleophilic attack by the 2′ oxygen from the 2′-OH group on the adjacent phosphorus atom, severing internucleotide linkage (19). The transesterification reaction occurs when the 5′-oxyanion leaving group is positioned directly at or 'in-line' with the opposing side of the target phosphorus center relative to the nucleophile (19–21). Therefore, internal RNA structures affect, as anticipated, the rate of the transesterification reaction (19). For this reason, in-line probing is a sensitive method to detect subtle structural difference in RNA without any chemical labeling of the RNA. As seen in Figure 2C, robust cleavage was observed in M2 but not in M1 in the regions of A49–A46 and of G37–G15. The difference in the in-line probing pattern covering a wide sequence range, i.e. A49–A46 and of G37–G15, suggested that the secondary (and tertiary) structure of M1 is quite different from M2 and that M1 might be folded to a greater complexity in its secondary and tertiary structures that were less prone to cleavage (19). Furthermore, internucleotide linkages near the ends of RNA are generally more susceptible to cleavage (22), presumably due to RNA fraying (23,24). In fact, M2 (and even M1) showed a greater tendency of fragmentation at both ends, as compared with its middle part of the structure. Surprisingly, however, the 3′-end region of SynAN58, i.e. C57–G55, exhibited a much stronger resistance to cleavage than both M1 and M2, despite the fact that M2 was generally similar in cleavage pattern to SynAN58. The structural uniqueness of the C57–G55 region in SynAN58 is currently unknown. However, the C57–G55 region was critical because deletion of the last five bases at the 3′-end, which covered this region, led to the total loss of inhibitory activity for either the synthetic RNA (i.e. SynAN53) or the enzymatic transcript of AN53

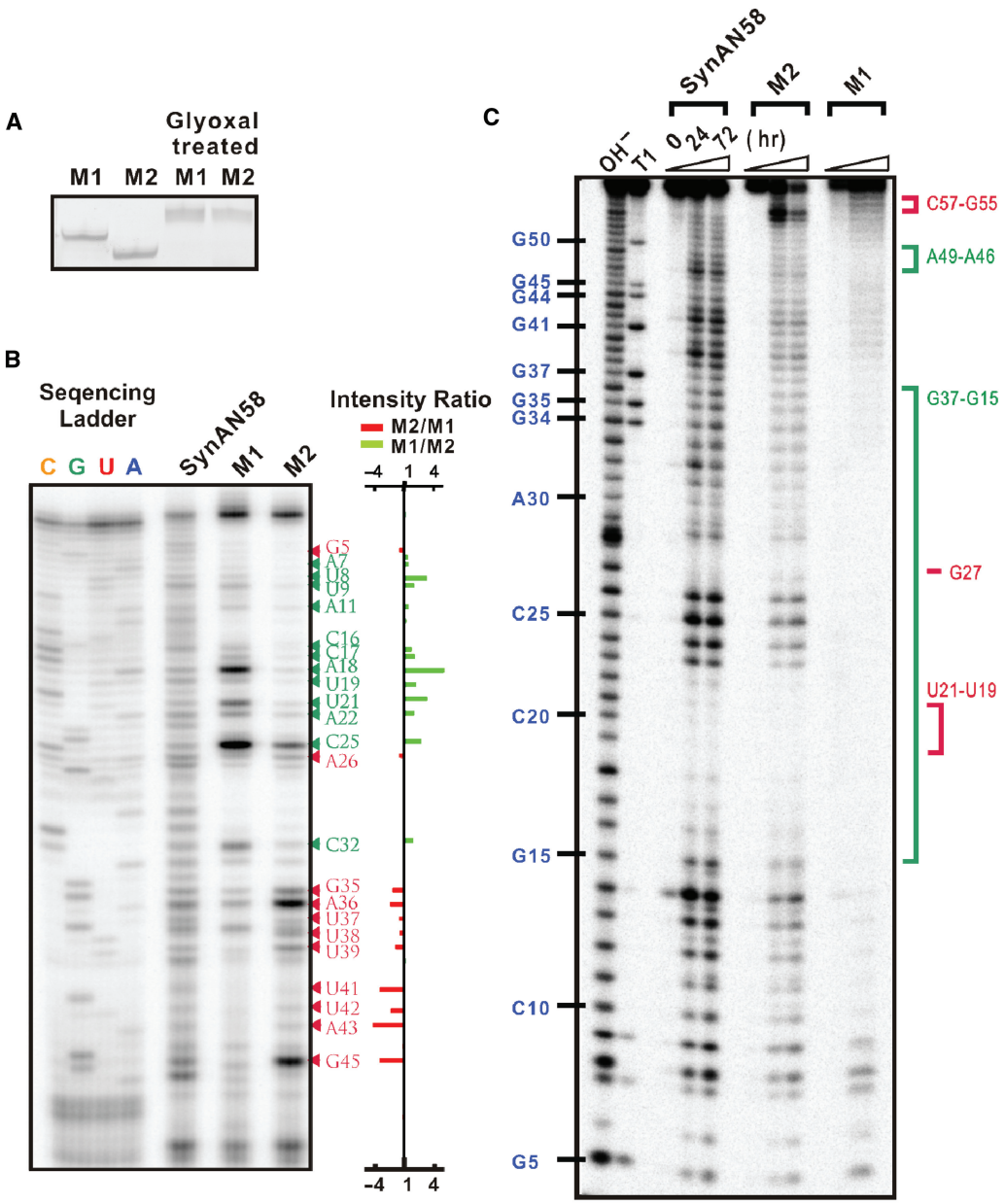

Figure 2. Structural differences in M1, M2 and SynAN58. (**A**) Glyoxal-treated M1 and M2 exhibited the same mobility in a 10% PAGE using a MOPS running buffer (20 mM MOPS or 3-(*N*-morpholino)propanesulfonic acid, 2 mM sodium acetate, 1 mM EDTA, pH 7.2). Without glyoxal treatment, M1 and M2 ran with different mobility under the same electrophoresis condition or even in denaturing PAGE (see Figure 4A, middle panel). (**B**) Primer extension of both M1 and M2 using a 5′-^{32}P-labeled 10-nt oligo primer. The four lanes on the left were sequencing ladders; and the SynAN58 was used as the control (middle lane). Shown on the right is a bar chart indicating the difference of RT stops in terms of the ratio of the intensity of radioactivity, which linked these stops to specific positions of the nucleotide in both M1 and M2. (**C**) In-line probing of M1 and M2. The first and the second lane were an alkaline hydrolysis ladder and an RNase T1 cutting ladder produced from SynAN58. All samples were kept in the external buffer (see the buffer composition in Materials and Methods) at 37°C for zero, 24 and 72 h as indicated (note that, although not shown, all of the samples could be eventually degraded completely or to single bases given enough time). The difference in the degradation pattern between M1 and M2 is marked in green color frame on the right. Similarly, the difference in the degradation pattern or the sequence region between SynAN58 and M2 is marked in red. All of the samples were 5′-end labeled and separated in a 12% sequencing PAGE containing 8 M urea.

(Figure 1D). Together, these results support the hypothesis that M1 and M2 can assume two distinct structural folds encoded by the same sequence. Furthermore, the synthetic AN58 seemed to have a structure different from either M1 or M2 despite the fact that SynAN58 shared the same sequence with the enzymatic transcripts M1 and M2 (Supplementary Figure 2).

SHAPE analysis of M1, M2 and SynAN58

The ribose 2′-hydroxyl group of an RNA is known to react with NMIA to form ester adducts at the 2′ position, but the acylation reactivity is influenced by the local structure such that a flexible nucleotide reacts with NMIA more readily than a nucleotide constrained by either base pairing or a tertiary interaction (13). Therefore, the

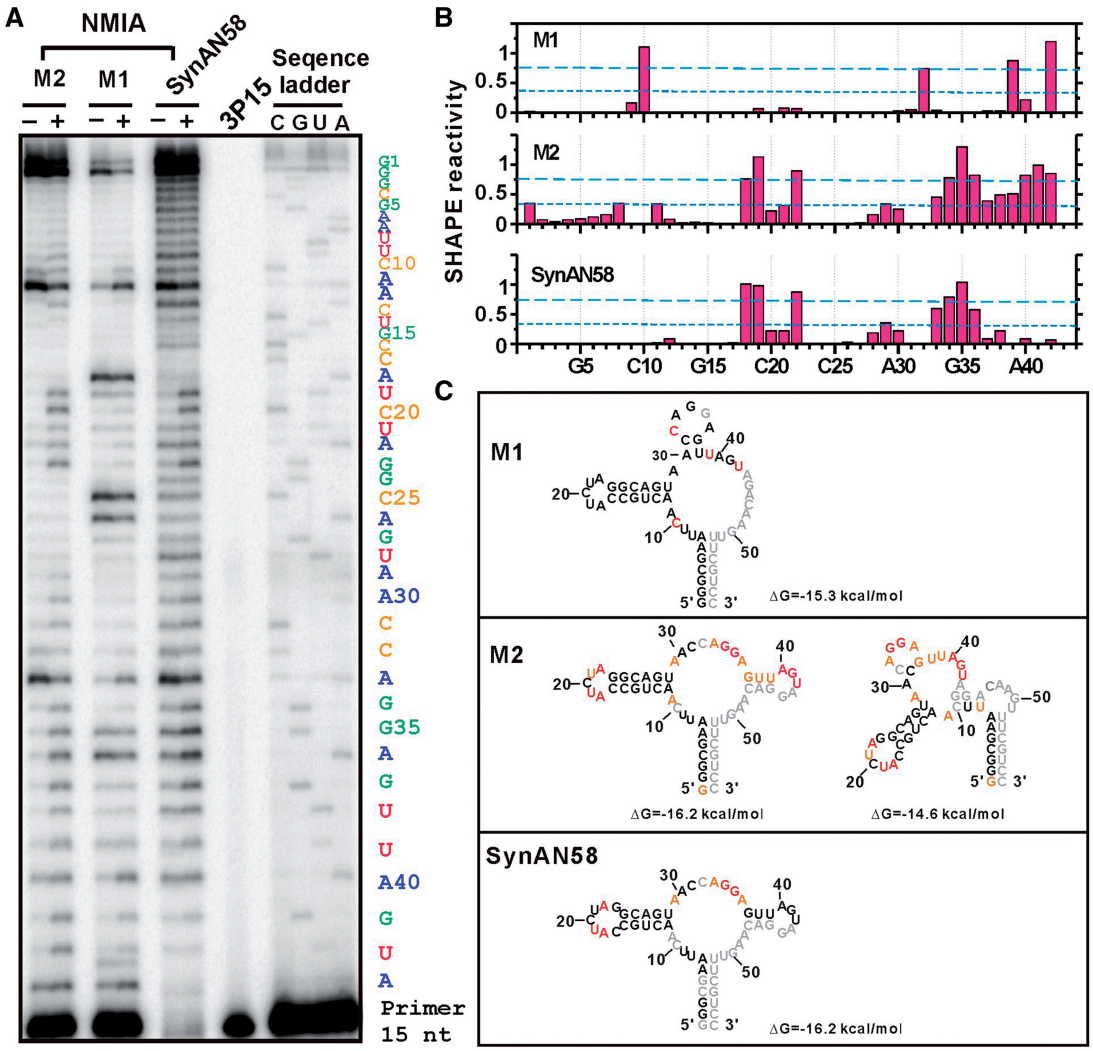

Figure 3. SHAPE analysis of M1, M2 and SynAN58. (**A**) The pattern of NMIA reactivity was probed by a reverse transcription reaction using a 5′-end, 15-nt oligo or 3P15, and visualized on a 12% denaturing PAGE containing 8 M urea. Other parameters were described in 'Materials and Methods' section. The sequencing ladder, shown on the right, was generated by dideoxy nucleotide incorporation during the primer extension, similar to Figure 2B. (**B**) Band intensity in the presence and absence of NMIA was quantified by using SAFA software (38). For each nucleotide position, the reactivity was calculated as the intensity difference between the NMIA labeled lane and the negative control lane; the negative control corresponded to a 10% DMSO (final concentration) in the same reaction mixture but without NMIA. There were also nucleotide positions where no reactivity could be detected or a negative reactivity was detected, due to strong RT stops in the absence of NMIA (Figure 2B). These positions, along with the last 15 nt for primer annealing, all marked in light gray in Figure 3C, were set to be zero in the reactivity value. The SHAPE reactivity score was calculated based on a method described previously (25,27). The long-dashed blue line indicates the threshold of 0.75 SHAPE reactivity score whereas the short-dashed line represents the threshold of 0.35 SHAPE reactivity score (see text for detailed explanation). (**C**) Secondary structures generated using RNAstructure (version 4.6) (26), based on the SHAPE reactivity score. The number of the structures displayed corresponded to those whose free energy differed by less than 10% from the lowest free energy in each of the structures.

reactivity of the acylation can be used to reveal locations of those conformationally dynamic nucleotides in an RNA. Experimentally, the reactivity can be detected by primer extension experiment because the formation of a 2′-ester adduct causes a RT stop (13). Using NMIA, we performed SHAPE experiment to probe the conformational dynamics of the structure for M1, M2 and SynAN58. Shown in Figure 3A is the gel electrophoresis analysis of the reactivity of NMIA at single nucleotide position up to nucleotide 43 (whereas the last 15 nt in the 58-nt RNA were covered by the primer annealing). The band intensities in the gels, which reflected RT stops, were quantified, using SAFA program, and the SHAPE reactivity for each species was calculated by a method previously described (25).

Based on the quantitative SHAPE reactivity (Figure 3B), both the overall number of nucleotides that were labeled and their respective positions were different for M1, M2 and SynAN58, consistent with the notion that each of the three species had a distinct structure. In particular, M1 had the least number of the nucleotide positions labeled overall. Furthermore, in the two major segments where both M2 and SynAN58 reacted prominently with NMIA, e.g. A18–A22 and A33–A36, the same nucleotides

in M1 exhibited no NMIA reactivity. In general, non-reactive nucleotides were thought to be Watson–Crick base-paired. A number of non-canonical base pairing, such as U–G, A–A and A–G, could also become nonreactive. We therefore concluded that a major network of base pairing and possibly tertiary interactions existed in M1, rendering only a few nucleotide residues solvent accessible. This conclusion is also consistent with result from the in-line probing experiment with M1 (Figure 2C), where a large portion of its structure showed considerable resistance to degradation on the same time scale, as compared with either M2 or SynAN58.

In contrast, the overall patterns of SHAPE reactivity between M2 and SynAN58 were similar (Figure 3B), suggesting the two were structurally similar. However, there were still clear differences. For instance, the SHAPE reactivity terminated at A36 for SynAN58, whereas it continued from G37–U42 for M2. This result indicated that the 3′-region may be the location that distinguishes M2 from SynAN58. Consistent with this result, the in-line probing experiment showed that M2 and SynAN58 had key structural difference in G55–C57 at the 3′-end (these nucleotides were not detectable in SHAPE experiment because they were part of the primer annealing site). It is further worth noting that in between G37–U42, SynAN58 showed no SHAPE reactivity, while M1 was labeled but only at U39 and U42, as compared to a broader reactivity in M2. Together, these results highlight the importance of the 3′-region in defining the uniqueness of the structures of these species.

Based on both the primary RNA sequence and more importantly the three sets of SHAPE reactivity scores (Figure 3B), we further predicted the secondary structures for M1, M2 and SynAN58, using an RNA structure prediction algorithm (26). The SHAPE reactivity was especially useful in the secondary structure prediction, because it provided experimental evidence to constrain the locations of the conformationally dynamic nucleotides (25). However, it should be noted that the following factors were taken into consideration in structural prediction (25,27). First, the reactivity score of 0.75 (i.e. the long-dashed line in Figure 3B and the nucleotides colored in red in Figure 3C) corresponded to the threshold of single-stranded, highly reactive nucleotide residues. The reactivity score between 0.75 and 0.35 (i.e. the short dashed-line in Figure 3B and the nucleotides colored in orange in Figure 3C) was considered to be those that were either base-paired or adjacent to bulges, mismatches, or G-U pairs, which could be more dynamic than nucleotides in the center of an uninterrupted helix. For the reactivity score below 0.35, however, the nucleotides were thought to be base-paired (25,27). According to these SHAPE reactivity constraints, the secondary structures were generated for M1, M2 and SynAN58 (Figure 3C). As seen (Figure 3C), their secondary structures are clearly different. For instance, in the constant region of the RNA aptamer or nucleotides of G1–C25 (6), a stem-loop was predicted (Figure 3C), supported by the SHAPE reactivity at some nucleotides in both M2 and SynAN58. However, the lack of NMIA reactivity in M1 roughly in the same loop position suggested that M1 might have a more complex structure involving with this region, such as its participating in a tertiary interaction. Furthermore, for both M1 and M2, there seemed to be another stem-loop near A40. However, such a region showed no SHAPE reactivity for SynAN58 (Figure 3C). The lack of the SHAPE reactivity near A40 for SynAN58 suggested a conformationally constrained local structure or is indicative of the involvement of this loop in a tertiary interaction.

M1 and M2, two non-convertible RNA folds

To begin to understand the structure-function relationship of the three RNA species, M1, M2 and their synthetic counterpart, SynAN58, we first asked whether M1 and M2 were interconvertible folds. If so, one species would be a transcription product whereas the other was the product of folding. To answer this question, we attempted to unfold and refold M1 and M2. However, even after boiling or ethanol precipitation or freezing, M1 and M2 remained individual bands, as visualized on native PAGE, and their biological activities also remained intact, as tested by whole-cell recording. After boiling in the presence of ~50% formamide for 15 min, M1 did partially unfold into a species that had mobility seemingly identical, on denaturing PAGE, to that of M2 (Figure 4A, the middle panel; the lower band of the M1). However, the lower band originating from the M1 sample disappeared upon refolding, suggesting that M1, under such a harsh denaturing condition, could partially unfold to some other structure(s) but not to M2. M2, on the other hand, appeared intact after such treatments as it remained a single band. We also attempted to denature M1 and M2 by raising solution pH to an extreme (28). In this experiment, a brief (i.e. 3 min) exposure of 10 mM NaOH (i.e. pH ~12) readily caused degradation or alkaline hydrolysis of both M1 and M2 but not denaturation or interconvertion from one to the other (Supplementary Figure 3). Based on these results, we concluded that M1 and M2 were not different conformers or products of folding/refolding. Instead, M1 and M2 were different structural entities assumed from the same sequence.

It should be noted that for drawing the conclusion as stated above, we also carried out a control experiment. Specifically, we constructed a 59-nt RNA producing plasmid (i.e. pRAV–AN59; see the 'Materials and Methods' section), which contained the *glmS* ribozyme sequence (9) linked to the 3′-end of the AN58 sequence. As the *glmS* ribozyme spliced between the AG sites (29), the 59-nt RNA that contained the AN58 aptamer sequence with an additional 'A' at the 3′-end was produced. As expected, the 59-nt RNA aptamer appeared as two bands at the similar positions on a native PAGE, which were similarly termed AN59 M1 and AN59 M2 (Figure 4B). Furthermore, AN59 M1 and AN59 M2 had identical length (see their LC–MS mass spectra in Supplementary Figure 4). More importantly, AN59 M1 and AN59 M2 exhibited the same properties as M1 and M2 (or AN58 M1 and M2) in that they were not interconvertible when subject to the same unfolding/refolding experiments (Figure 4B), yet they had inhibitory function identical

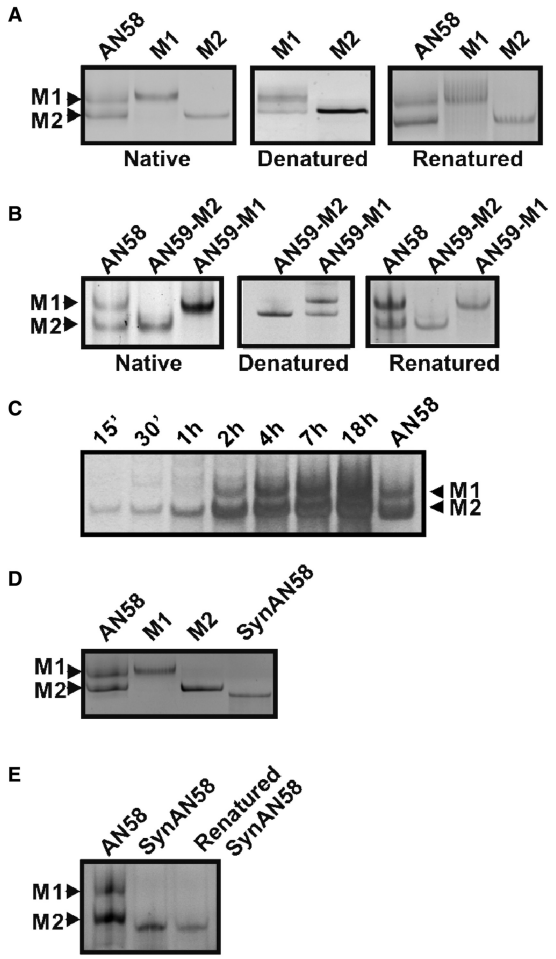

Figure 4. M1 and M2, the two nonconvertible RNA folds. (**A**) Unfolding and refolding of AN58 M1 and M2. The left panel shows the different mobility of purified M1 and M2 in a native PAGE (10%), compared with the mixture of the original sample, AN58. When the purified M1 and M2 dissolved in the Loading Buffer II (Ambion) for denaturing PAGE, which contained 47.5% formamide (final concentration), were boiled for 15 min and run in the denaturing PAGE (10%, 7 M urea), additional band appeared originating from the M1 sample (middle panel). The "denatured" M1 and M2 were then precipitated in ethanol and re-suspended in the external buffer; the refolded samples were visualized in another native PAGE (10%) (right panel). Note that in the same native PAGE, the AN58 sample was treated by the same unfolding/refolding process. The M1 and M2 used in the folding/refolding experiments were also purified to remove the contaminated acrylamide (see 'Materials and Methods' section). (**B**) The same unfolding and refolding experiment and gel electrophoresis as described in (A) but with AN59 M1 and AN59 M2. The AN59 aptamer was generated by using pRAV23 plasmid, and cleaved by *glmS* ribozyme (see 'Materials and Methods' section). (**C**) The time course of M1 and M2 transcription as visualized in a 10% native PAGE by ethidium bromide staining. The transcription reaction was carried out at 37°C, and the samples from different time points were taken as shown. The line labeled as AN58 was the transcription product from a 12 h reaction. (**D**) The chemically synthesized AN58 or SynAN58 showed an electrophoretic mobility different from either AN58 M1 or AN58 M2. (**E**) The same unfolding and refolding experiment and gel electrophoresis as described in (A) but with SynAN58.

to AN58 M1/M2, evidenced by the finding that as a pair, but not alone, AN59 M1 and AN59 M2 acted as an inhibitor on GluR2Q_{flip} AMPA receptors and with an identical inhibitory potency to the AN58 M1/M2 pair (data not shown). This control experiment demonstrated that the functional and structural difference between M1 and M2 were not attributed to the possibility of an uneven length between M1 and M2.

It is possible, however, that M1 and M2, regardless of AN58 or AN59 version, might be folded and refolded in their own repertoires of conformations or folding networks (at least this may be true for M1), there is not a thermodynamic pathway through which a conformation from one conformational repertoire can become the origin of the other conformational repertoire (i.e. the so-called conformational diffusion between the two networks) (1). Although we cannot rule out that there may be yet an unidentified denaturing condition under which M1 and M2 can both be denatured post-transcriptionally, the conditions used in this study are to our knowledge the strongest denaturing conditions known. The lack of an apparent pathway through which M1 and M2 can be interconverted by unfolding and refolding or refolding after denaturation suggests an unusual folding landscape with an energy barrier that is sufficiently high to irreversibly separate the two different structures. Thus the structural differences between M1 and M2 seem not to be a result of RNA-folding process or conformational partitioning (1,30).

Co-transcriptional formation of M1 and M2

Our finding that M1 and M2 are not different folds that can be reversibly formed or interconverted post-transcriptionally by any unfolding/refolding pathway suggests that both M1 and M2, rather than just one species, should be enzymatic products of *in vitro* transcription, as observed (Figures 1A and 2A). Furthermore, our results also suggest that the two structural entities, i.e. M1 and M2, are generated during the transcription or are co-transcriptional products. Characteristic of an enzymatic reaction, both the rate and the yield of the transcription reaction of M1 and M2 were shown to depend on temperature and Mg^{2+} concentration (see Figure 4C and also Supplementary Figure 5). Interestingly, the transcription rate of M2 was always faster than M1 (Figure 4C and Supplementary Figure 5). How M1 and M2 are formed during transcription is currently not known. One possibility is the existence of a nascent knot or a topologically entangled helix formed during the transcription perhaps for one or both species, which may set M1 and M2 apart. The interhelical stacking on a basis of a three-way junction, as in the case of the hammerhead ribozyme, could provide additional stability through base pairing between the two closing loops of helices (31). Such a structure is known to be stable even in as low an Mg^{2+} concentration as 100 μM (32). In our case, the M1 and M2, once folded during transcription, were stable either alone or together even at zero concentration of Mg^{2+}. It should be also emphasized that M1 and M2 were both the transcription reaction products generated in the presence of the T7 RNA polymerase, because M1 and M2 were generated despite the fact that T7 RNA polymerases from different sources, e.g. Ambion transcription kit, and purified wild type, were used. Furthermore, when the DNA

template was replaced with the SynAN58 RNA, which was then subject to a transcription reaction with T7 RNA polymerase, SynAN58 remained intact, namely, it did not convert to either M1 or M2 (Supplementary Figure 6). Together, these results show that M1 or M2 is not a chemically modified product by any potentially contaminating sources such as another enzyme, etc., in the transcription reaction; rather, M1 and M2 were the transcription products from the T7 RNA polymerase-catalyzed reaction. However, it should be noted that these results did not rule out the possibility of a chemical modification of one or both transcripts by T7 RNA polymerase during the transcription reaction. Such a chemical modification is possible given the extraordinary stability of these two species, which made it impossible, at least with known denaturing agents, to unfold them.

The synthetically made AN58 or SynAN58 was different from AN58 M1 and M2 in several ways. First, SynAN58 appeared as a *single* band in native PAGE and exhibited a different mobility from either the M1 or the M2 (Figure 4D). SynAN58 had a different RT pause pattern in the reverse transcription reaction (Figure 2B) and a different in-line probing profile (Figure 2C) from either the M1 or the M2, although by and large SynAN58 was more similar to the AN58 M2 (Figures 2C and 3B). Furthermore, SynAN58 inhibited the GluR2 AMPA receptor with an inhibition constant being ~4-fold lower than transcriptionally generated AN58 or the mixture of M1 and M2 (6). The apparent differences in both the function and the structure between the synthetically made AN58 and enzymatic products, although all shared the same sequence, may be due to the possibility that the folding of an RNA during transcription is known to occur sequentially from the 5′-end to the 3′-end of an RNA molecule. The directionality of the transcription, together with the speed of the transcription reaction, may create an order of the folding events different from the refolding of the full-length RNA with the same sequence (33,34). The fact that SynAN58 does not fold into either M1 or M2, even after SynAN58 was subject to the same denaturation/refolding treatment (Figure 4E) as in AN58 M1/M2 (Figure 4A) and AN59 M1/M2 (Figure 4B), is further consistent with the hypothesis that M1 and M2 are co-transcriptional products. Presently, studies using chemical and enzymatic probing as well as structural techniques, together with mutational analysis, are ongoing to refine the secondary structures and to probe the tertiary structures for the three species.

DISCUSSION

The results from this study provide interesting implications to the evolution of RNA structure and function in nature. As shown in Figure 4A, for example, it was not possible to unfold/refold the AN58 M1 and M2 post-transcriptionally, and consequently the M1 and M2 were not able to convert to each other, despite the fact that the M1 and M2 were assumed from the same sequence. However, as shown (Figure 2B), both the M1 and M2 could be *fully* reverse-transcribed in spite of different RT pauses during elongation. This result suggested that reverse transcriptase was the 'denaturant' to 'melt' the RNA during the *in vitro* evolution (6). Then the prediction could be made that running separate reverse transcription/PCR reactions for M1 and M2, the two non-convertible RNA isolates, followed by two separate *in vitro* transcriptions, would yield both M1 and M2 as transcription products, independent of the input RNA template. In fact, this was exactly what we found (Supplementary Figure 7). This result further suggested that the original, full-length sequence of AN58 or aptGluR2-99 that contained the functional M1 and M2 domains would be expectedly capable of surviving phenotypic selection, which required reverse transcription in each SELEX cycle. Clearly, the evolution of the aptamer sequence (genotype) was driven by the selection of that aptamer (desired genotype) for its binding to receptor (35). In fact, AN58 and aptGluR2-99 were both shown to bind to the extracellular glutamate-binding domain (or the S1S2 protein) assayed by radio-ligand binding and were both functionally active as inhibitors of the GluR2 AMPA receptor assayed by whole-cell recording (6).

The results described above suggested that the survival and evolution of one phenotype (selectable shape), such as the M1-containing RNA, was enough to ensure the concurrent survival of the other phenotype or the M2-containing aptamer, because the two phenotypes are encoded by the same genotype (replicable sequence). Here evolution can be viewed as a walk over the set of genotypes preferring 'fitter' offspring (36). In our case, because the two phenotypes are not conformers that are reversibly interconvertible and because both are selected with distinct functions, both of them are therefore fitter. The ability of the same genotype to encode two phenotypes during the course of evolution is surprisingly and profoundly meaningful in that the two phenotypes, both of which are apparently very stable and functionally useful (as part of the inhibitory pair), must survive through a shared evolution origin and history. It would be otherwise almost impossible or too fortuitous that two phenotypes could have been selected against all odds among a vast number of possible RNA molecules or selectable shapes. Thus, our results suggest more broadly that natural RNA molecules can evolve to acquire alternative structures and associated functions that are genealogically linked by even one phenotype.

The transfer of *sequence information* between two different classes of nucleic acids is not generally considered difficult because such a process uses the one-to-one correspondence of Watson–Crick pairing (37). However, the transfer of *function* is difficult because function is a property of a macromolecule that is inherently more complex than sequence. In a recent study, it was shown that the evolutionary conversion of a ribozyme (RNA) to a deoxyribozyme (DNA) of the same function can be accomplished but only with some critical sequence mutations (37). The finding from this study shows that the survival of one genotype can entail more than one phenotype through *in vitro* evolution, suggesting that transfer of different functions through the same sequence from DNA to RNA is possible. Furthermore, it is perhaps not surprising that the structures assumed from the same sequence

formed during transcription must be so stable thermodynamically as to ensure the integrity of a particular function. Therefore RNA may be more phenotypically adaptable than proteins, given the fact that unlike RNA, a real protein does not unify genotype and phenotype in one molecule (36). Currently, no protein sequence is known to fold autonomously into two different structures endowing two functions (2). Therefore, our results support the hypothesis (2), albeit in a different way, that RNAs that show structural dissimilarities with different functions can nevertheless share a common ancestry and bear the same evolution memory. It is possible that in a real organism a single RNA sequence could evolve to 'duplicate' RNA molecules with structure-dependent functional dissimilarities, which, in some cases, may precede gene duplication.

SUPPLEMENTARY DATA

Supplementary Data are available at NAR Online.

ACKNOWLEDGEMENTS

We thank John Lis (Cornell University) for his generous and insightful advices and help during the course of this project. We thank Ronald Breaker, Adam Roth (Yale University) and Phil Sharp (MIT) for helpful discussion and advices. We thank Robert Batey and Jeffrey Kieft (University of Colorado) for kindly providing the pRAV23 vector. We acknowledge Gang Li in the lab for some data collection.

FUNDING

Department of Defense grant (W81XWH-04-1-0106 to L.N.), National Institutes of Health grant (R01NS060812 to L.N.), the ALS Association grant (to L.N.), Muscular Dystrophy Association grant (to L.N.); postdoctoral fellowship from Muscular Dystrophy Association (to Z.H.). Funding for open access charge: Department of Defence.

Conflict of interest statement. None declared.

REFERENCES

1. Huynen,M.A., Stadler,P.F. and Fontana,W. (1996) Smoothness within ruggedness: the role of neutrality in adaptation. *Proc. Natl Acad. Sci. USA*, **93**, 397–401.
2. Schultes,E.A. and Bartel,D.P. (2000) One sequence, two ribozymes: implications for the emergence of new ribozyme folds. *Science*, **289**, 448–452.
3. Mandal,M. and Breaker,R.R. (2004) Gene regulation by riboswitches. *Nat. Rev. Mol. Cell Biol.*, **5**, 451–463.
4. Tuerk,C. and Gold,L. (1990) Systematic evolution of ligands by exponential enrichment: RNA ligands to bacteriophage T4 DNA polymerase. *Science*, **249**, 505–510.
5. Ellington,A.D. and Szostak,J.W. (1990) In vitro selection of RNA molecules that bind specific ligands. *Nature*, **346**, 818–822.
6. Huang,Z., Pei,W., Jayaseelan,S., Shi,H. and Niu,L. (2007) RNA aptamers selected against the GluR2 glutamate receptor channel. *Biochemistry*, **46**, 12648–12655.
7. Hollmann,M. and Heinemann,S. (1994) Cloned glutamate receptors. *Annu. Rev. Neurosci.*, **17**, 31–108.
8. Dingledine,R., Borges,K., Bowie,D. and Traynelis,S.F. (1999) The glutamate receptor ion channels. *Pharmacol. Rev.*, **51**, 7–61.
9. Batey,R.T. and Kieft,J.S. (2007) Improved native affinity purification of RNA. *RNA*, **13**, 1384–1389. Epub 2007 Jun 1384.
10. Winkler,W.C., Nahvi,A., Roth,A., Collins,J.A. and Breaker,R.R. (2004) Control of gene expression by a natural metabolite-responsive ribozyme. *Nature*, **428**, 281–286.
11. McMaster,G.K. and Carmichael,G.G. (1977) Analysis of single- and double-stranded nucleic acids on polyacrylamide and agarose gels by using glyoxal and acridine orange. *Proc. Natl Acad. Sci. USA.*, **74**, 4835–4838.
12. Sambrook,J. and Rusell,D.W. (2001) *Molecular Cloning, A Laboratory Manual*, 3rd edn. Cold Spring Harbor Laboratory Press, New York, pp. 7.27–7.30.
13. Wilkinson,K.A., Merino,E.J. and Weeks,K.M. (2005) RNA SHAPE chemistry reveals nonhierarchical interactions dominate equilibrium structural transitions in tRNA(Asp) transcripts. *J. Am. Chem. Soc.*, **127**, 4659–4667.
14. Li,G., Pei,W. and Niu,L. (2003) Channel-opening kinetics of GluR2Q(flip) AMPA receptor: a laser-pulse photolysis study. *Biochemistry*, **42**, 12358–12366.
15. Li,G., Oswald,R.E. and Niu,L. (2003) Channel-opening kinetics of GluR6 kainate receptor. *Biochemistry*, **42**, 12367–12375.
16. Honore,T., Davies,S.N., Drejer,J., Fletcher,E.J., Jacobsen,P., Lodge,D. and Nielsen,F.E. (1988) Quinoxalinediones: potent competitive non-NMDA glutamate receptor antagonists. *Science*, **241**, 701–703.
17. Harrison,G.P., Mayo,M.S., Hunter,E. and Lever,A.M. (1998) Pausing of reverse transcriptase on retroviral RNA templates is influenced by secondary structures both 5′ and 3′ of the catalytic site. *Nucleic Acids Res.*, **26**, 3433–3442.
18. Klasens,B.I., Huthoff,H.T., Das,A.T., Jeeninga,R.E. and Berkhout,B. (1999) The effect of template RNA structure on elongation by HIV-1 reverse transcriptase. *Biochim. Biophys Acta.*, **1444**, 355–370.
19. Soukup,G.A. and Breaker,R.R. (1999) Relationship between internucleotide linkage geometry and the stability of RNA. *RNA*, **5**, 1308–1325.
20. Celander,D.W. and Cech,T.R. (1991) Visualizing the higher order folding of a catalytic RNA molecule. *Science*, **251**, 401–407.
21. Cate,J.H. and Doudna,J.A. (1996) Metal-binding sites in the major groove of a large ribozyme domain. *Structure*, **4**, 1221–1229.
22. Usher,D.A. and McHale,A.H. (1976) Hydrolytic stability of helical RNA: a selective advantage for the natural 3′,5′-bond. *Proc. Natl Acad. Sci. USA*, **73**, 1149–1153.
23. Jin,R., Chapman,W.H. Jr, Srinivasan,A.R., Olson,W.K., Breslow,R. and Breslauer,K.J. (1993) Comparative spectroscopic, calorimetric, and computational studies of nucleic acid complexes with 2′,5′-versus 3′,5′-phosphodiester linkages. *Proc. Natl Acad. Sci. USA*, **90**, 10568–10572.
24. Puglisi,E.V., Puglisi,J.D., Williamson,J.R. and RajBhandary,U.L. (1994) NMR analysis of tRNA acceptor stem microhelices: discriminator base change affects tRNA conformation at the 3′ end. *Proc. Natl Acad. Sci. USA*, **91**, 11467–11471.
25. Wilkinson,K.A., Gorelick,R.J., Vasa,S.M., Guex,N., Rein,A., Mathews,D.H., Giddings,M.C. and Weeks,K.M. (2008) High-throughput SHAPE analysis reveals structures in HIV-1 genomic RNA strongly conserved across distinct biological states. *PLoS Biol.*, **6**, e96.
26. Mathews,D.H., Disney,M.D., Childs,J.L., Schroeder,S.J., Zuker,M. and Turner,D.H. (2004) Incorporating chemical modification constraints into a dynamic programming algorithm for prediction of RNA secondary structure. *Proc. Natl Acad. Sci. USA*, **101**, 7287–7292.
27. Mortimer,S.A. and Weeks,K.M. (2007) A fast-acting reagent for accurate analysis of RNA secondary and tertiary structure by SHAPE chemistry. *J. Am. Chem. Soc.*, **129**, 4144–4145.
28. Doty,P., Boedtker,H., Fresco,J.R., Haselkorn,R. and Litt,M. (1959) Secondary Structure in Ribonucleic Acids. *Proc. Natl Acad. Sci. USA*, **45**, 482–499.
29. Roth,A., Nahvi,A., Lee,M., Jona,I. and Breaker,R.R. (2006) Characteristics of the glmS ribozyme suggest only structural roles for divalent metal ions. *RNA*, **12**, 607–619.

30. Herschlag,D. (1995) RNA chaperones and the RNA folding problem. *J. Biol. Chem.*, **270**, 20871–20874.
31. Khvorova,A., Lescoute,A., Westhof,E. and Jayasena,S.D. (2003) Sequence elements outside the hammerhead ribozyme catalytic core enable intracellular activity. *Nat. Struct. Biol.*, **10**, 708–712.
32. Schroeder,R., Barta,A. and Semrad,K. (2004), *Nat. Rev. Mol. Cell Biol.*, **5**, pp. 908–919.
33. Lewicki,B.T., Margus,T., Remme,J. and Nierhaus,K.H. (1993) Coupling of rRNA transcription and ribosomal assembly in vivo. Formation of active ribosomal subunits in Escherichia coli requires transcription of rRNA genes by host RNA polymerase which cannot be replaced by bacteriophage T7 RNA polymerase. *J. Mol. Biol.*, **231**, 581–593.
34. Pan,T., Fang,X. and Sosnick,T. (1999) Pathway modulation, circular permutation and rapid RNA folding under kinetic control. *J. Mol. Biol.*, **286**, 721–731.
35. Spiegelman,S. (1971) An approach to the experimental analysis of precellular evolution. *Q. Rev. Biophys.*, **4**, 213–253.
36. Bornberg-Bauer,E. (1997) How are model protein structures distributed in sequence space? *Biophys. J.*, **73**, 2393–2403.
37. Paul,N., Springsteen,G. and Joyce,G.F. (2006) Conversion of a ribozyme to a deoxyribozyme through in vitro evolution. *Chem. Biol.*, **13**, 329–338.
38. Das,R., Laederach,A., Pearlman,S.M., Herschlag,D. and Altman,R.B. (2005) SAFA: semi-automated footprinting analysis software for high-throughput quantification of nucleic acid footprinting experiments. *RNA*, **11**, 344–354.